*Korean J. Chem. Eng.*, 39(7), 1768-1774 (2022)
DOI: 10.1007/s11814-022-1109-0

pISSN: 0256-1115
eISSN: 1975-7220

# Chitosan-based porous carbon as a support for Zn-based catalysts in acetylene acetoxylation

**Junyu Zhang*, Fulong Zhu*, Ying Zhang*, Mingyuan Zhu*,**,†, Hongling Li*,†, and Bin Dai***

*School of Chemistry and Chemical Engineering of Shihezi University, Shihezi, Xinjiang 832003, P. R. China
**College of Chemistry & Chemical Engineering of Yantai University, Yantai, Shandong, 264010, P. R. China
(*Received 13 December 2021 • Revised 11 March 2022 • Accepted 14 March 2022*)

**Abstract**−Using the biomass material chitosan as a precursor and potassium citrate (PC) as a substitute for traditional corrosive activators such as KOH and $ZnCl_2$, a chitosan-based porous carbon material with high specific surface area was successfully prepared and used as a support for the catalytic acetylene acetoxylation reaction. By controlling the PC content and the calcination temperature, chitosan-based porous carbon with a suitable pore structure and abundant surface oxygen functional groups was obtained. The inductively coupled plasma analysis confirmed that the zinc content of the 0.9Zn/CS-$PC_1$-800 catalyst was about 14 wt%, and the acetic acid conversion reached 81%. Furthermore, the scanning electron microscopy and Brunauer-Emmett-Teller (BET) analysis showed that the catalyst carrier was mesoporous carbon material, and different PC content formed different pore size distribution at different calcination temperatures. In addition, X-ray photoelectron spectroscopy analysis demonstrated that the content of O in chitosan-based porous carbon was rich, and PC consumed the O content on the surface of carbon materials during activation. Because O content and pore size structure on carrier surface are closely related to acetic acid conversion, reasonable PC content and calcination temperature are very important for acetic acid conversion.

Keywords: Chitosan-based Porous Carbon, Potassium Citrate, Oxygen Functional Groups, Acetylene Acetoxylation, Zn-based Catalysts

## INTRODUCTION

Vinyl acetate (VAc) is an important chemical raw material, mainly used in the production of ethylene-vinyl acetate (EVA) and polyvinyl alcohol (PVA) [1] VAc is extensively used in a various of fields, including paints [2], aviation [3], construction [4], medicine [5], and soil improvement. At present, VAc is mainly produced via the acetylene ($C_2H_2$) method in China due to its rich coal resources.

In this reaction, the order of activity of metallic components is Hg>Bi>Cd>Zn. However, among the available catalysts, zinc acetate has attracted much attention because of its low cost, ease of manufacture, and good performance in the $C_2H_2$ acetoxylation reaction. In the industrial version of this reaction, zinc acetate is adsorbed on activated carbon (AC) by impregnation as a catalyst [6].

However, using AC as a support presents a series of drawbacks such as low conversion of acetic acid ($CH_3COOH$) and fast deactivation of the catalyst. According to the rational mechanism of $C_2H_2$ acetoxylation [7], $CH_3COOH$ combines with the active component and then reacts with the adsorbed $C_2H_2$ to produce ethylene acetate while zinc acetate is reduced. However, the adsorption capacity of Zn is stronger for $C_2H_2$ than for $CH_3COOH$, and abundant $C_2H_2$ occupies more active sites, resulting in reduced activity and instability of the catalyst. Therefore, to improve the adsorption performance of the catalyst for $CH_3COOH$, bimetallic catalysis and heteroatomic doping have been extensively studied. For example, He et al. [8] found that the addition of bimetal considerably improves the catalyst performance; the conversion of $CH_3COOH$ increased by ten percentage points, and N doping could change the electron cloud density of Zn. Wu et al. [9] used cyanide to modify AC with N and found that the $CH_3COOH$ conversion of N-doped AC catalyst was improved. Zhu et al. prepared B-doped AC catalyst. The introduction of B atom enhance the electron transfer and adsorption capacity between Zn and $CH_3COOH$, and effectively increased the conversion of $CH_3COOH$ from 50% to 65%. By changing the contents of -COOH and -OH on the AC surface, Zhu et al. [10] proved that adding -COOH into the dicarboxylic catalytic system could enhance the adsorption capacity of the active component over $C_2H_2$ in the reaction process, thus improving the conversion of $CH_3COOH$. However, a high $CH_3COOH$ conversion could not be achieved; therefore, a high-performance catalyst carrier still needs to be developed.

In recent years, the use of polymer materials extracted from biomass, such as cellulose, lignin, and chitosan, to prepare carbon-based catalysts has attracted extensive attention due to their remarkable advantages in terms of nontoxicity, biodegradability, and biocompatibility [11,12]. Biochar has been widely used in catalysis, especially as a carrier for metals, owing to its wide range of raw material precursors, low cost, large surface area (high dispersion and stability of metallic phases), and stability in alkaline and acidic media, among other favorable physical/chemical surface properties [13].

In particular, chitosan, a kind of renewable natural biomass with low cost and high O and N content, is a potential raw material for

†To whom correspondence should be addressed.
E-mail: zhuminyuan@shzu.edu.cn, lhl_tea@shzu.edu.cn

the synthesis of carbon materials [14]. Carbon materials made from directly carbonized of biomass materials usually have a relatively simple pore structure and relatively low specific surface area, which is of interest because the construction of a porous structure is an effective way to obtain high-performance catalysts. Traditionally, porous carbon is mainly produced via the template method using hard and soft templates, which requires activation of the carbon materials to form hierarchical pore structures [15,16]. To this aim, several chemical activators (such as KOH, $K_2CO_3$ and $ZnCl_2$) have been widely used; however, these compounds are highly corrosive [17-21]. In recent years, potassium citrate (PC), a neutral potassium compound, has emerged as a more benign alternative for the preparation of microporous AC [22-24].

In this study, chitosan-based porous AC was prepared by hydrothermal activation method using PC as an activator instead of corrosive KOH. By adjusting the mass ratio of PC and the activation temperature, various AC materials with different specific surface areas and surface oxygen contents were prepared as catalyst carriers, and Zn-based catalysts with high performance were obtained.

## MATERIALS AND EXPERIMENTAL

### 1. Chemicals

Deionized water (FBZ1002-SUP, Fulemu Qingdao, China) was used as the solvent for this experiment. chitosan (MW=300,000), PC ($C_6H_5K_3O_7$), KOH, $K_2C_2O_4$, $K_2CO_3$, $CH_3COOH$ (Yongsheng Tianjin, China, 99.5%), zinc acetate (Aldrich, 99.8%), and $C_2H_2$ (Weichuang gas Urumqi, China, 99.99%) used in the experiment were all analytical grade materials.

### 2. Preparation of Porous Carbon

The chitosan-based porous carbon materials (CS-$PC_X$) were synthesized as follows: First, 30 g chitosan was mixed with 400 mL deionized water under mechanical stirring, and the mixture was then added into 30 mL $CH_3COOH$, producing a homogeneous thick solution. Next, the thick solution was put into an autoclave lined with Teflon and hydrothermally carbonized for 150 min at 200 °C. The brownish black powders collected by vacuum filtration were washed with deionized water until neutral and then dried at 90 °C overnight. After that, the powders were impregnated with the activation agent at different mass ratios of powder to activation agent (X=0, 0.5, 1, 2) and stirred for 10 h at 25 °C. Subsequently, the samples were dried at 110 °C until moisture was completely removed. The CS-$PC_X$ materials were obtained after carbonization under flowing $N_2$ at 400 °C for 2 h at a heating rate of 5 °C/min, followed by heating at different temperatures to find the optimum conditions (700 °C, 800 °C, 900 °C) at a rate of 5 °C/min. The mixture was maintained at that temperature for an additional 2 h. The resultant materials were washed with a 2 M HCl solution and distilled water until neutral. After drying at 90 °C overnight, the CS-$PC_X$-700, CS-$PC_X$-800, and CS-$PC_X$-900 products were obtained.

### 3. Preparation of the Catalysts

Zinc acetate (1 g) was dissolved in 30 mL deionized water and stirred at room temperature for 30 min. Then, CS-$PC_1$-800 by (3 g) was added and stirred at 25 °C for 10 h and 80 °C for another 12 h until dry. The resulting catalyst was named as 0.3Zn/CS-$PC_1$-800, where 0.3 represents the mass ratio of zinc acetate to carbon carrier, 1 represents the mass ratio of PC to chitosan, and 800 represents the calcination temperature in °C.

### 4. Catalytic Performance Test

The $C_2H_2$ acetoxylation reaction was performed in a fixed bed reactor with a 1.2 cm stainless steel tube. The catalyst (0.6 g) was put into the reactor and heated to 200 °C under $N_2$ atmosphere. Then, a peristaltic pump was used to continuously pump the $CH_3COOH$ preheated at 150 °C to activate the catalyst, and the reaction temperature was adjusted to 220 °C. After heating at 220 °C for 30 min, $N_2$ was replaced with pure $C_2H_2$ (10 mL/min), and the gas volume flow ratio of $C_2H_2$ to $CH_3COOH$ was 3 : 1. For the analysis of the products, a Shimadzu GC-9A gas chromatograph and an N2000 chromatographic data station (double channel) were used.

### 5. Catalyst Characterization

A scanning electron microscope (SEM; TESCAN MIRA4) was used to investigate the microstructure of the as-obtained products. Brunauer-Emmett-Teller (BET) analysis was conducted using a Micromeritics ASAP 2460 apparatus at −196 °C. Raman spectra were recorded on a Horiba Scientific LabRAM HR Evolution instrument. X-ray photoelectron spectroscopy (XPS) analysis was conducted utilizing a Thermo Scientific K-Alpha apparatus (hv=1,486 eV). The metal elements were determined by Inductively coupled plasma emission spectrometry (ICP-OES).

## RESULTS AND DISCUSSION

Chitosan porous carbon materials treated with different activators (PC, $K_2C_2O_4$, $K_2CO_3$, KOH) were selected as catalyst carriers, and their properties were tested after the same content of zinc acetate was loaded on these carriers. As shown in Fig. S1, the catalytic performance of the catalysts treated with the four activators is slightly different, among which the catalyst Zn/CS-PC activated by potassium citrate has the best catalytic performance. Therefore, we used chitosan as carbon source and potassium citrate as activator for further study.

Details of the porous structure of the supports are summarized in Table 1. The specific surface area of CS-$PC_0$-800 was only 8.57 $m^2\ g^{-1}$, and a clear increase to 1,451.2 $m^2\ g^{-1}$ for CS-$PC_1$-800 was observed with the addition of PC. The total pore volume of CS-$PC_1$-800 was 0.78 $cm^3\ g^{-1}$. However, upon further increasing the PC content in CS-$PC_2$-800, no change in either the specific surface area or the pore size was observed. Meanwhile, the specific surface area of the CS-$PC_1$ samples increased with the temperature. It can be seen that PC as an activator changes the specific surface area and

**Table 1. Pore structure information of the supports**

| Sample | Surface area ($m^2\ g^{-1}$) | Pore size (nm) | Pore volume ($cm^3\ g^{-1}$) |
|---|---|---|---|
| CS-$PC_0$-800 | 8.57 | 8.45 | 0.02 |
| CS-$PC_{0.5}$-800 | 843.17 | 2.01 | 0.42 |
| CS-$PC_1$-800 | 1,451.24 | 2.14 | 0.78 |
| CS-$PC_2$-800 | 1,430.8 | 2.14 | 0.77 |
| CS-$PC_1$-700 | 1,080.81 | 2.05 | 0.55 |
| CS-$PC_1$-900 | 1,603.41 | 2.05 | 0.82 |

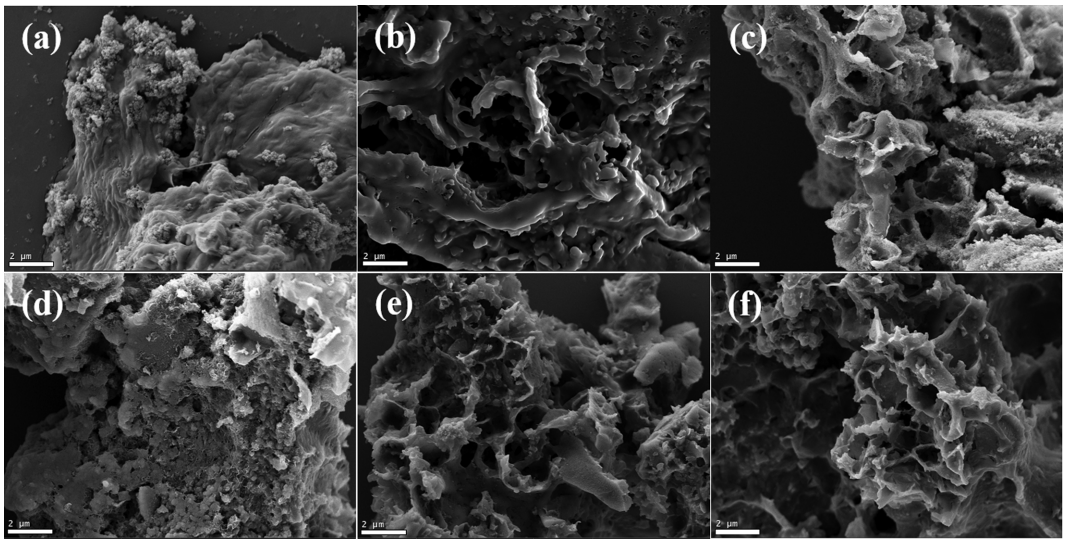


**Fig. 1. Scanning electron microscopy images of the synthesized catalysts: (a) CS-PC$_0$-800, (b) CS-PC$_{0.5}$-800, (c) CS-PC$_1$-800, (d) CS-PC$_2$-800, (e) CS-PC$_1$-700 and (f) CS-PC$_1$-900.**

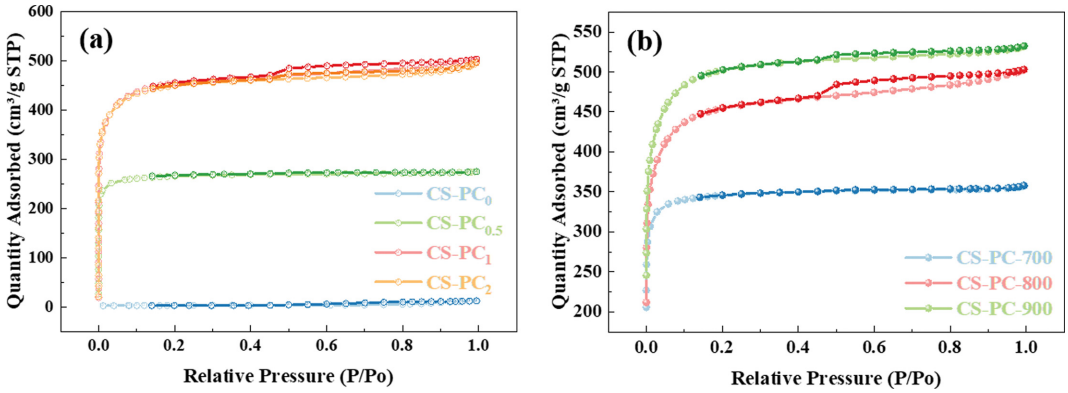


**Fig. 2. $N_2$ adsorption-desorption isotherms of the supports at (a) different PC content and (b) different temperature.**

pore size structure.

To further explore the role of PC at different conditions, the surface morphology of the CS-PC$_0$-800, CS-PC$_{0.5}$-800, CS-PC$_1$-800, CS-PC$_2$-800, CS-PC$_1$-700, and CS-PC$_1$-900 samples was investigated via SEM, and the results are displayed in Fig. 1. The SEM images of nonactivated chitosan-based carbon (CS-PC$_0$; Fig. 1(a)) showed a small number of folds and particles of various microns, with irregular morphology. Moreover, no obvious aperture was observed. The SEM images of CS-PC$_{0.5}$-800, CS-PC$_1$-800 and CS-PC$_2$-800 (Fig. 1(b), (c) and (d)) showed that the activation of PC resulted in the formation of stratified pores with sizes ranging from several nanometers to microns on the SEM surface of the samples. The activated samples, CS-PC$_1$-800 and CS-PC$_2$-800 showed higher porosity and more open holes than CS-PC$_{0.5}$-800. The porosity of CS-PC$_1$-800 and CS-PC$_2$-800 can effectively increase the surface area of the support. The SEM images of the CS-PC$_1$-700 and CS-PC$_1$-900 samples (Fig. 1(e) and (f)) revealed that porous carbon materials were formed at 700 °C and 900 °C. To further investigate the activation effect of the PC content and the calcination temperature on the pore structure, $N_2$ adsorption-desorption isotherms were recorded (Fig. 2(a) and (b)).

As shown in Fig. 2(a) and (b), $N_2$ adsorption-desorption isotherms of the porous carbon carriers exhibited both type I (a sharp increase at low relative pressure indicating rich micropores) and type IV (an obvious hysteresis loop at medium relative pressure indicating the existence of mesopores) characteristics, which suggests a well-developed hierarchical porous structure according to the IUPAC classification [25]. These results are consistent with the results of the SEM measurements. The $N_2$ adsorption level of the CS-PC$_1$-800 and CS-PC$_2$-800 samples was significantly higher than that of CS-PC$_0$-800 and CS-PC$_{0.5}$-800, which can be attributed to the presence of abundant pores in the former samples. Compared with other samples, CS-PC$_1$-800 and CS-PC$_1$-900 exhibited an obvious hysteresis loop, indicating that the formation of mesopores was related to the activator and the carbonization temperature.

To investigate the defects and graphitization of the prepared supports, Raman spectra of the supports fabricated with different proportions and temperatures were recorded, and the results are shown in Fig. 3(a) and (b). All the spectra showed two independent peaks at ca. 1,360 and ≈1,589 cm$^{-1}$, which can be assigned to defective and

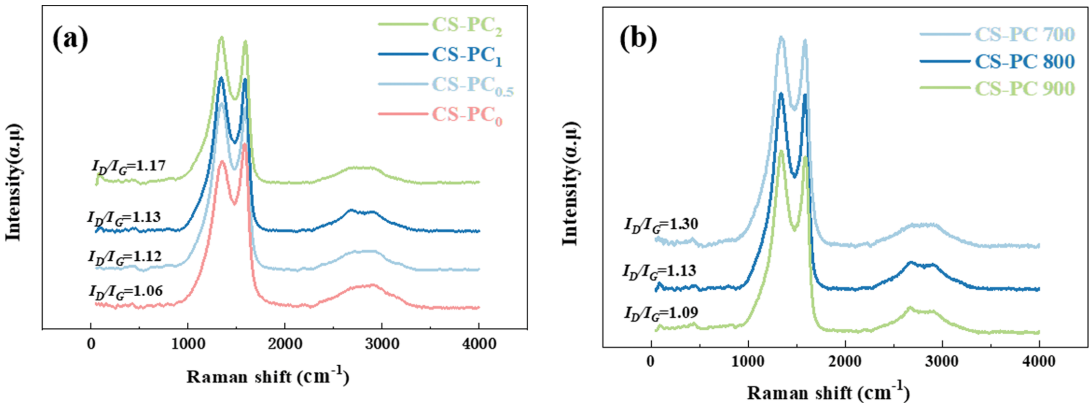


**Fig. 3. Raman spectra of (a) CS-PC$_X$ (X=0, 0.5, 1, 2) and (b) CS-PC$_1$-700, CS-PC$_1$-800 and CS-PC$_1$-900.**

ordered graphite, respectively [26]. Furthermore, the relative degree of defects in the carbon materials was estimated according to the strength ratio $I_D/I_G$, which was determined to be 1.06, 1.12, 1.13, 1.17, 1.30, and 1.09 for CS-PC$_0$-800, CS-PC$_{0.5}$-800, CS-PC$_1$-800, CS-PC$_2$-800, CS-PC$_1$-700, and CS-PC$_1$-900, respectively. After the addition of PC, the $I_D/I_G$ ratio of CS-PC$_X$ increased from 1.06 to 1.17, indicating that the number of defects increased, which is consistent with the increase in the BET specific surface area. Moreover, the $I_D/I_G$ value decreased from 1.30 for CS-PC$_1$-700 to 1.09 for CS-PC$_1$-900 upon increasing the temperature, indicating that the graphitization degree increased most likely due to the removal of amorphous carbon or other impurities [27].

By comparing Table 2 and Table 1, it can be seen that the zinc acetate loading had a significant impact on the pore structure of the CS-PC$_X$ carrier. The specific surface area of CS-PC$_1$-800 was reduced by approximately 22.4%, from 1,451.2 to 1,126.1 m$^2$ g$^{-1}$. In addi-

**Table 2. Pore structure information of the catalysts**

| Sample | Surface area ($m^2$ $g^{-1}$) | Pore size (nm) | Pore volume ($cm^3$ $g^{-1}$) |
|---|---|---|---|
| Zn/CS-PC$_0$-800 | 3.73 | 16.19 | 0.02 |
| Zn/CS-PC$_1$-800 | 1,126.13 | 2.12 | 0.58 |
| Zn/CS-PC$_2$-800 | 976.64 | 2.18 | 0.53 |
| Zn/CS-PC$_1$-900 | 1,103.65 | 2.10 | 0.58 |

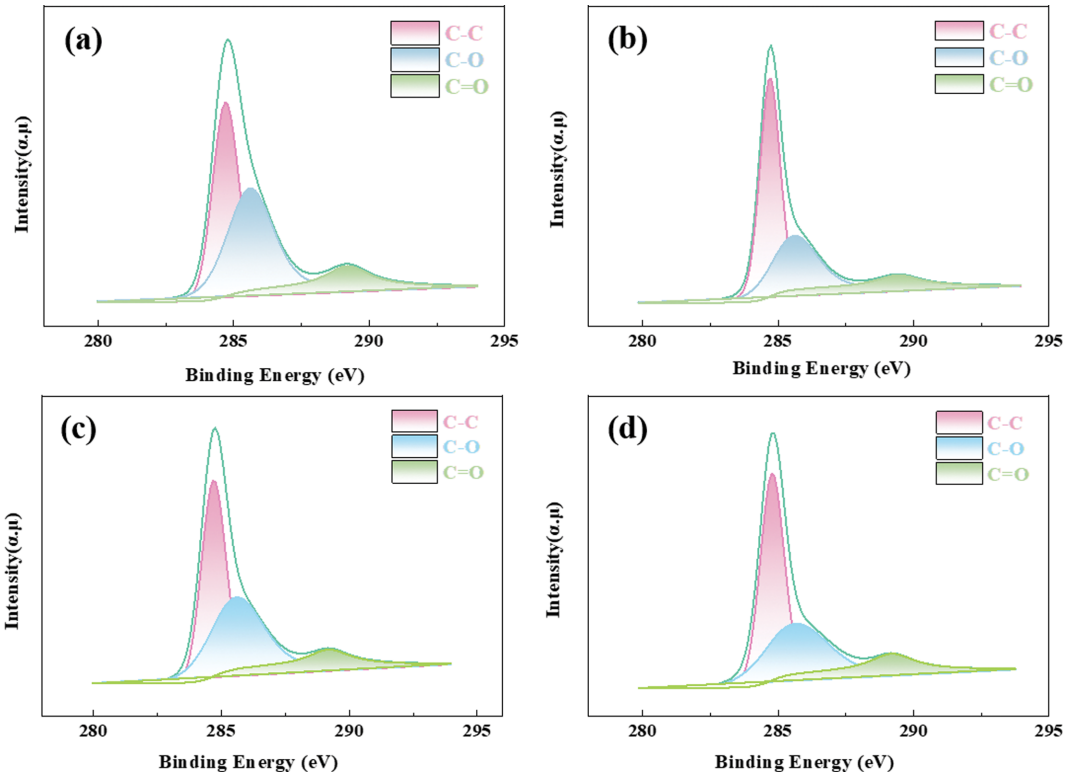


**Fig. 4. X-ray photoelectron C1s spectrum of (a) Zn/CS-PC$_1$-800, (b) Zn/CS-PC$_2$-800, (c) Zn/CS-PC$_1$-700 and (d) Zn/CS-PC$_1$-900.**

**Table 3. Total O, N, and oxygen-containing functional groups contents of different carriers calculated by XPS analysis**

| Sample | Contents atomic% | | C=O | C-O |
|---|---|---|---|---|
| | O | N | | |
| Zn/CS-PC$_1$-800 | 14.52 | 1.03 | 0.122 | 0.454 |
| Zn/CS-PC$_2$-800 | 9.32 | 0.95 | 0.095 | 0.384 |
| Zn/CS-PC$_1$-700 | 14.58 | 1.16 | 0.122 | 0.457 |
| Zn/CS-PC1-900 | 11.05 | 0.85 | 0.098 | 0.421 |

tion, a significant change in the pore volume of CS-PC$_1$-800 from 0.78 to 0.58 cm$^3$ g$^{-1}$ was observed. The results show that a suitable channel structure was formed in the supports and the catalysts and no rock-ribbed channel blockage phenomenon occurred; the active component was successfully loaded.

XPS measurements were used to evaluate the effect of the elemental composition on the surface of the carbon materials, as shown in Fig. 4 and Table 3. To gain a deeper understanding of the surface functional groups of the samples, the C1s XPS spectra of Zn/CS-PC$_1$-800, Zn/CS-PC$_2$-800, Zn/CS-PC$_1$-700, and Zn/CS-PC$_1$-900 were deconvoluted into three peaks (Fig. 4(a), (b), (c) and (d)). The strong peak at a binding energy of 284.6 eV corresponds to the carbon atom located in the graphite ring (C-C), and the strong peak at 285.5 eV can be assigned to the carbon atom attached to an oxygen atom (C-O). In addition, the wide and low-intensity deconvolution peak at a binding energy of 289.2 eV corresponds to ester and carboxyl groups (C=O) [28].

The presence of N can improve the adsorption capacity of the catalyst for $CH_3COOH$, thereby enhancing the conversion. As shown in Table 3, there is little difference in the total N content among the catalysts; therefore, the effect of the N content in the performance can be ignored. The total oxygen content and C=O content of Zn/CS-PC$_1$-800 was 14.52% and 0.122, respectively. However, with the increase in the PC content, the total oxygen content and C=O content of Zn/CS-PC$_2$-800 decreased to 9.32% and 0.095, indicating that PC consumed O, especially C=O, in the etching process. Meanwhile, the total oxygen content and C=O content decreased with increasing the calcination temperature, especially for Zn/CS-PC$_1$-900.

Compared with Zn/CS-PC$_1$-800, the total oxygen content of Zn/CS-PC$_1$-900 decreased by 24% (from 14.52% to 11.05%) and the C=O content decreased by 20% (from 0.122% to 0.098%). According to these results, PC consumed a certain amount of O in the carbon materials during the activation process. Therefore, the Zn/CS-PC$_1$-800 and Zn/CS-PC$_2$-800 catalysts having the same pore size exhibited the best performance.

First, the stability of catalyst in reaction was studied. It can be observed from Fig. S2 that the XPS peak of zinc has not been shifted by X-ray photoelectron Zn 2p spectral analysis of fresh and used catalysts, so we believe that zinc still exists in the form of zinc acetate after the reaction. TGA and DTG analysis of 0.9Zn/CS-PC$_1$-

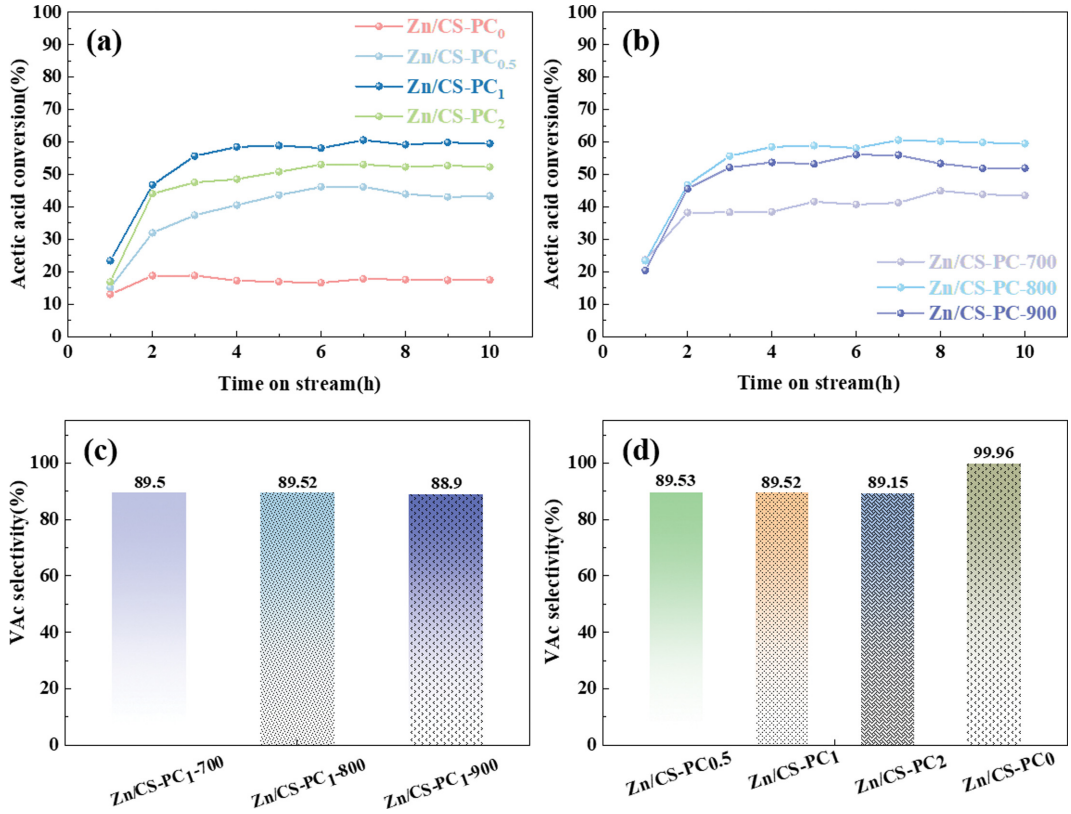


**Fig. 5. Conversion of $CH_3COOH$ (a) over Zn/CS-PC$_X$ catalysts with different ratios of potassium citrate and chitosan and (b) catalysts obtained at different calcination temperatures. The selectivity of VAc (c) over Zn/CS-PC$_X$ catalysts with different ratios of potassium citrate and chitosan and (d) catalysts obtained at different calcination temperatures.**

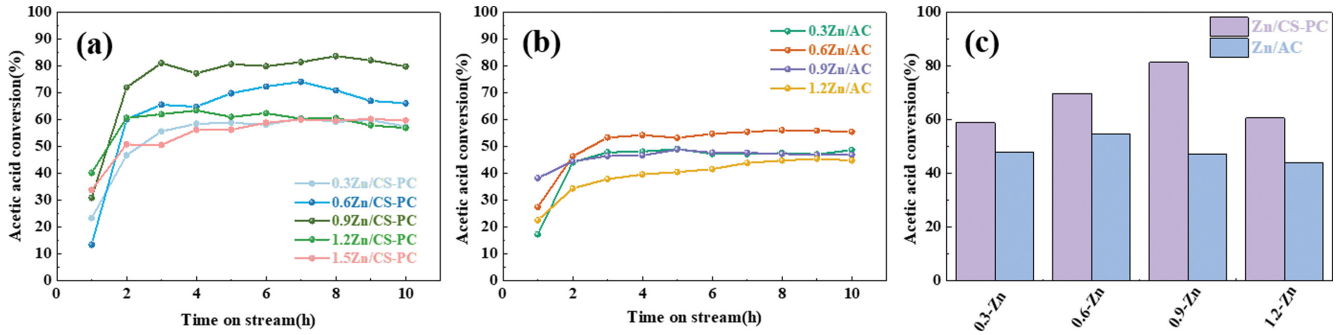


**Fig. 6. Conversion of $CH_3COOH$ over (a) Zn/CS-PC and (b) Zn/AC catalysts with different Zn loading. (c) Relationship between the Zn content and the $CH_3COOH$ conversion.**

**Table 4. Zn content (wt%) of different catalysts**

| Catalyst | Actual loading (wt%) | |
|---|---|---|
| | Zn | K |
| 0.3 Zn/CS-$PC_1$-800 | 6.50 | 0.260 |
| 0.6 Zn/CS-$PC_1$-800 | 10.55 | 0.260 |
| 0.9 Zn/CS-$PC_1$-800 | 14.31 | 0.235 |
| 1.2 Zn/CS-$PC_1$-800 | 16.14 | 0.295 |

800 catalyst are shown in Fig. S3. It is clear that the mass of catalyst loses 2.7% at 100 °C, and decreases by 1.2% at 220 °C, indicating that the catalyst is relatively stable at the reaction temperature.

Next, the performance of the catalysts in the $C_2H_2$ acetoxylation reaction was investigated. First, as can be seen from Fig. 5(a), the conversion of $CH_3COOH$ increased gradually with the PC ratio. When the mass ratio of PC to chitosan was 1, the conversion of $CH_3COOH$ was the highest (ca. 59.8%). In a certain range, the conversion of acetic acid is proportional to the specific surface area and C=O content of the carrier. Then, using the optimal ratio of PC and chitosan, the calcination temperature of the carrier was optimized. A carrier with high specific surface area and high C=O content was obtained. As can be extracted from Fig. 5(b), Zn/CS-$PC_1$-800 outperformed Zn/CS-$PC_1$-700 and Zn/CS-$PC_1$-900, revealing that the former was the best catalyst. It is clear from Fig. 5(c) and 5(d) that the selectivity of vinyl acetate is about 89%. The other by-products are acetone and crotonaldehyde.

Finally, the Zn content of the catalysts was optimized under the conditions of a mass ratio of PC to chitosan of 1 and a calcination temperature of 800 °C. The $CH_3COOH$ conversion under different Zn loadings is depicted in Fig. 6(a). According to Table 4, when the Zn content increased to a certain extent, the $CH_3COOH$ conversion reached its maximum value. The Zn content in the catalysts was determined via ICP-OES (Table 4). When the Zn content reached 14 wt%, the CS-$PC_1$-800 carrier had the best loading capacity and the $CH_3COOH$ conversion reached 81%. However, the $CH_3COOH$ conversion decreased significantly when the Zn content was excessive. In general, the optimum reaction conditions were as follows: Zn loading of 14 wt%, a mass ratio of PC to chitosan of 1, and a calcination temperature of the carrier of 800 °C. Compared with the conversion of $CH_3COOH$ over AC with different Zn loadings (Fig. 6(b)), the performance of the Zn/$N_2$ catalyst was significantly improved, as can be clearly observed in Fig. 6(c).

## CONCLUSIONS

Chitosan-based hierarchical porous carbon materials were prepared using chitosan as carbon source and PC as an activator via a one-pot heat treatment method, and a series of Zn-based catalysts were fabricated via a simple impregnation method using the as-prepared carbon materials. The porous carbon material obtained by optimizing the PC to chitosan ratio and the calcination temperature was used as a carrier for $C_2H_2$ acetoxylation catalysts. By selecting the ratio of PC and chitosan and optimizing the appropriate calcination temperature, the porous carbon material CS-$PC_1$-800 can be used as a carrier of acetylene acetoxylation catalyst. The $CH_3COOH$ conversion of Zn/CS-PC was 81% when Zn loading was 14 wt%, which was significantly higher than that of traditional Zn/AC catalyst. It was because potassium citrate regulated the oxygen-containing functional groups and pore structures on the surface of carbon materials. Within a certain range, the conversion rate is proportional to the specific surface area and the content of oxygen-containing functional groups. Overall, this study provides a new platform for the development of $C_2H_2$ acetoxylation catalysts.

## ACKNOWLEDGEMENTS

This work was supported by the State Key Research and Development Project of China (2016YFB0301603), the National Natural Science Funds of China (NSFC, 22178225) and the Taishan Scholars Program of Shandong Province (tsqn202103051).

## CONFLICT OF INTEREST

The authors declare that they have no known competing financial interests or personal relationships that could have appeared to influence the work reported in this paper.

## SUPPORTING INFORMATION

Additional information as noted in the text. This information is available via the Internet at http://www.springer.com/chemistry/journal/11814.

## REFERENCES


1. C. Nakason, W. Kaewsakul and A. Kaesaman, *J. Elastomers Plast.*, **44**, 89 (2012).
2. A. Yuliestyan, A. A. Cuadri, M. García-Morales and P. Partal, *Rheol. Acta*, **57**, 71 (2018).
3. S. P. Tambe, S. K. Singh, M. Patri and D. Kumar, *Prog. Org. Coat.*, **62**, 382 (2008).
4. A. Acosta, E. Gallio, P. Zanatta, H. Schulz, R. d. A. Delucis and D. Gatto, *Fibers Polym.*, **22**, 745 (2021).
5. E. Marques and P. J. Mancha, *Med. Phys.*, **45**, 1715 (2018).
6. H. Schobert, *Chem. Rev.*, **114**, 1743 (2014).
7. B. A. Morrow, *J. Catal.*, **86**, 328 (1984).
8. P. He, L. Huang, X. Wu, Z. Xu, M. Zhu, X. Wang and B. Dai, *Catalysts*, **8**, 239 (2018).
9. X. Wu, P. He, X. Wang and B. Dai, *Chem. Eng. J.*, **309**, 172 (2017).
10. F. Zhu, J. Li, M. Zhu and L. Kang, *Nanomaterials*, **11**, 1174 (2021).
11. M. Zahedifar, A. Es-Haghi, R. Zhiani and S. M. Sadeghzadeh, *RSC Adv.*, **9**, 6494 (2019).
12. R. S. Varma, *ACS Sustainable Chem. Eng.*, **9**, 6494 (2019).
13. S. Abdullah, N. Hanapi, A. Azid, R. Umar and H. Juahira, *Renewable Sustainable Energy Rev.*, **70**, 1040 (2016).
14. K. Chen, S. Weng, J. Lu, J. Gu, G. Chen, O. Hu, X. Jiang and L. Hou, *Micropor. Mesopor. Mater.*, **320**, 111106 (2021).
15. X. Yongde, Y. Zhuxian and M. Robert, *Nanoscale*, **2**, 639 (2010).
16. J. Jin, S. Tanaka, Y. Egashira and N. Nishiyama, *Carbon*, **48**, 1985 (2010).
17. C. Dai, J. Wan, J. Yang, S. Qu, T. Jin, F. Ma and J. Shao, *Appl. Surf. Sci.*, **444**, 105 (2018).
18. T. Ouyang, T. Zhang, H. Wang, F. Yang, J. Yan, K. Zhu, K. Ye, G. Wang, L. Zhou, K. Cheng and D. Cao, *Chem. Eng. J.*, **352**, 459 (2018).
19. M. Rajesh, R. Manikandan, S. Park, B. C. Kim, W.-J. Cho, K. H. Yu and C. J. Raj, *Int. J. Energy Res.*, **44**, 8591 (2020).
20. J. Shao, F. Ma, G. Wu, C. Dai, W. Geng, S. Song and J. Wan, *Chem. Eng. J.*, **321**, 301 (2017).
21. L. Zhang, T. You, T. Zhou, X. Zhou and F. Xu, *ACS Appl. Mater. Interfaces*, **8**, 13918 (2016).
22. J. Gao, L. Li, Z. Zeng, X. Ma, R. Chen, C. Wang and K. Zhou, *J. Mater. Sci.*, **54**, 6186 (2019).
23. X. Luo, S. Li, H. Xu, X. Zou, Y. Wang, J. Cheng, X. Li, Z. Shen, Y. Wang and L. Cui, *J. Colloid Interface Sci.*, **582**, 940 (2021).
24. L. Hou, W. Yang, Y. Li, P. Wang, B. Jiang, C. Xu, C. Zhang, G. Huang, F. Yang and Y. Li, *Chem. Eng. J.*, **417**, 129289 (2021).
25. J. Y. Bai, L. J. Wang, Y. J. Zhang, C. F. Wen, X. L. Wang and H. G. Yang, *Appl. Catal., B*, **266**, 118590 (2020).
26. S. Tian, J. Dai, Y. Jiang, Z. Chang, A. Xie, J. He, R. Zhang and Y. Yan, *J. Colloid Interface Sci.*, **505**, 858 (2017).
27. X.-Y. Yu, T. Luo, Y.-X. Zhang, Y. Jia, B.-J. Zhu, X.-C. Fu, J.-H. Liu and X.-J. Huang, *ACS Appl. Mater. Interfaces*, **3**, 2585 (2011).
28. A. M. Puziy, O. I. Poddubnaya, R. P. Socha, J. Gurgul and M. Wisniewski, *Carbon*, **46**, 2113 (2008).

# Supporting Information

# Chitosan-based porous carbon as a support for Zn-based catalysts in acetylene acetoxylation

**Junyu Zhang*, Fulong Zhu*, Ying Zhang*, Mingyuan Zhu*,**,†, Hongling Li*,†, and Bin Dai***

*School of Chemistry and Chemical Engineering of Shihezi University, Shihezi, Xinjiang 832003, P. R. China
**College of Chemistry & Chemical Engineering of Yantai University, Yantai, Shandong, 264010, P. R. China
(*Received 13 December 2021 • Revised 11 March 2022 • Accepted 14 March 2022*)

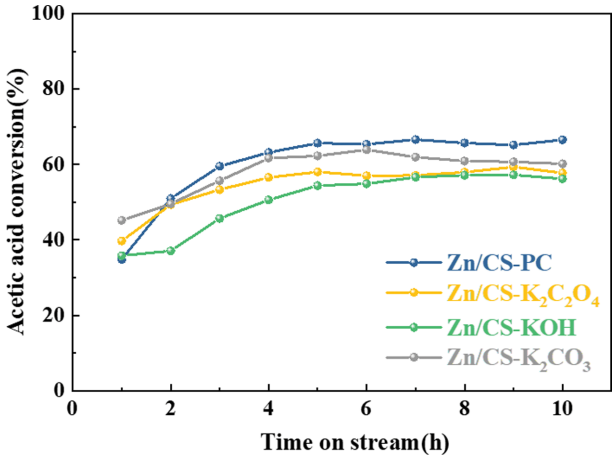


**Fig. S1. $CH_3COOH$ conversion of catalyst treated with different activators.**

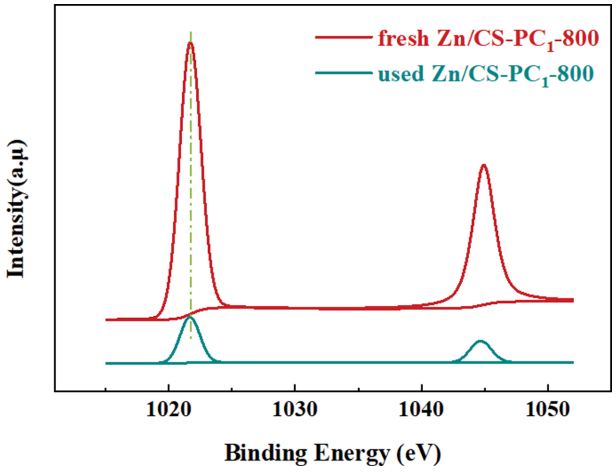


**Fig. S2. X-ray photoelectron Zn2p spectroscopic analysis of fresh and used Zn/CS-PC1-800 catalysts.**

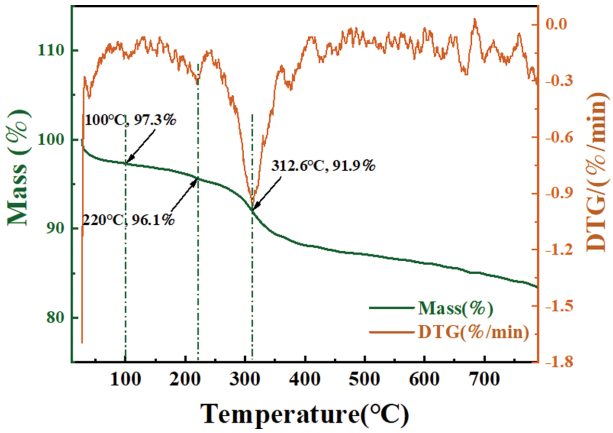


**Fig. S3. Thermogravimetric (TGA) and derivative thermogravimetric (DTG) analysis of 0.9Zn/ CS-PC1-800 catalyst.**